Lab on a Chip

Accepted Manuscript

ROYAL SOCIETY OF CHEMISTRY

www.rsc.org/loc

Graphical Abstract

A new, miniaturized chemical sensor – implanted via needle biopsy – measures tissue pH and oxygen tension *in vivo*.

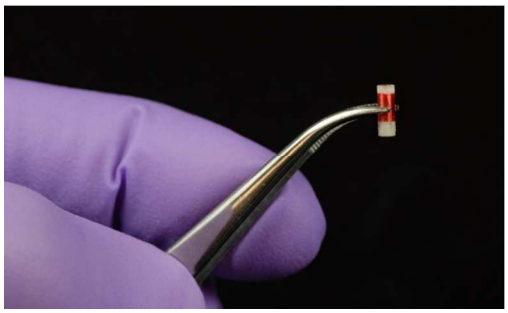

Journal Name

ARTICLE

Miniaturized, biopsy-implantable chemical sensor with wireless, magnetic resonance readout

Received 00th January 20xx,
Accepted 00th January 20xx

DOI: 10.1039/x0xx00000x

www.rsc.org/

C. C. Vassiliou,[a,b†] V. H. Liu,[a,b] and M. J. Cima[a,c]

Biopsy is an important diagnostic tool for a broad range of conditions. Cancer diagnoses, for example, are confirmed using tissue explanted with biopsy. Here we demonstrate a miniaturized wireless sensor that can be implanted during a biopsy procedure and return chemical information from within the body. Power and readout are wireless via weak magnetic resonant coupling to an external reader. The sensor is filled with responsive nuclear magnetic resonance (NMR) contrast agents for chemical sensitivity, and on-board circuitry constrains the NMR measurement to the contents. This sensor enables longitudinal monitoring of the same location, and its simple readout mechanism is ideal for applications not requiring the spatial information available through imaging techniques. We demonstrated the operation of this sensor by measuring two metabolic markers, both *in vitro* and *in vivo*: pH in flowing fluid for over 25 days and in a xenograft tumor model in mice, and oxygen in flowing gas and in a rat hind-limb constriction experiment. The results suggest that this *in vivo* sensing platform is generalizable to other available NMR constrats agents. These sensors have potential for use in biomedicine, environmental monitoring and quality control applications.

Introduction

Magnetic resonance imaging (MRI) is unparalleled in its ability to non-invasively peer into the physiology of living organisms. MRI can selectively image different compartments within the body, and a wealth of contrast agents allow highlighting of specific physiological structures[1]. Chemically-sensitive contrast agents, meanwhile, can report on the spatial distribution of clinically-relevant markers. These molecular imaging agents are injected systemically in sufficient concentration to provide contrast at the site of interest [2–5]. Obtaining quantitative results with these agents is challenging because they are quickly cleared from the body, and partitioning into particular tissue compartments is difficult to quantify. This rapidly changing concentration level must be accounted for through specialized pulse sequences or molecular design[6,7] and long-term monitoring requires multiple injections[8]. A needle probe with a chemically sensitive tip can monitor biomarker activity at the region of interest, but the measurements are invasive precluding their use for routine long-term monitoring. Repeat measurements on a heterogeneous tissue will also be confounded by this heterogeneity and it will be impossible to attribute measured changes to that occurring over time versus heterogeneity across the tissue[9,10]. Leaving a wired probe implanted introduces the risk of infection, and many probes require calibration between measurements.

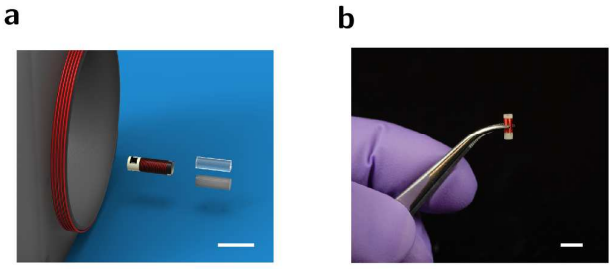

Figure 1 The three components of the sensing system are shown in **a**. The reader coil on the left is 28 mm in diameter, the implantable sensor is in the middle and the two contrast agents are on the right. The oxygen sensor is a clear silicone whereas the pH sensor is a white gel. A photo of the prototype sensor (**b**). The scale bars are 5 mm.

Two options for local, long-term monitoring with NMR are retention of the NMR contrast agent in a capsule or embedding of the agent in a solid matrix[11–14]. These approaches ensure a constant concentration at the site of interest, reduce the amount of contrast agent needed, and always monitor the same position. They require, however, an MRI scanner for *in vivo* measurements.

[a] *Koch Institute for Integrative Cancer Research,*
[b] *Department of Electrical Engineering and Computer Science, and*
[c] *Department of Materials Science and Engineering, Massachusetts Institute of Technology, Cambridge, MA 02139, USA.*
† Present address: Department of Chemistry, University of California, Berkeley, CA 94720

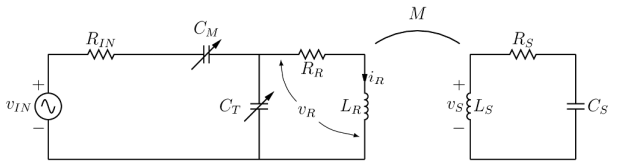

Figure 2 Circuit diagram of the reader (left) coupled to the sensor (right) via mutual inductance between the two inductances. The variable capacitors C_M and C_T ensure proper impedance matching to the spectrometer at the NMR precession frequency. The resistances model losses in the coils.

We have designed and constructed a system consisting of an implantable nuclear magnetic resonance (NMR) sensor and an external reader that operates without need for a MRI scanner. The sensor encloses a chemically-sensitive contrast agent and has an on-board circuit that communicates with an external reader (Fig. 1a). The complete sensor (Fig. 1b) is small enough to be implanted during a routine biopsy procedure and is designed to reside inside the body to repeatedly measure the same location. The sensor is interrogated wirelessly via weak magnetic coupling to a reader, which resides outside the body. The measurement is restricted to the contents of sensor by amplification provided by the on-board resonant circuit; this property allows different targets to be sensed by simply switching the sensitive contrast agent.

We demonstrate the flexibility of the implantable NMR sensor by separately detecting pH and oxygen tension *in vitro* and *in vivo* with appropriately chosen contrast agents. These two quantities were chose as they are clinically important for many conditions, such as being indicators of prognosis and treatment efficacy in cancer[15,16]. They cannot be measured in the systemic circulation and long-term temporal monitoring is important for the treatment of cancer, because a clinician could monitor chemical changes in the tumor after a treatment is administered and adjust therapy accordingly.

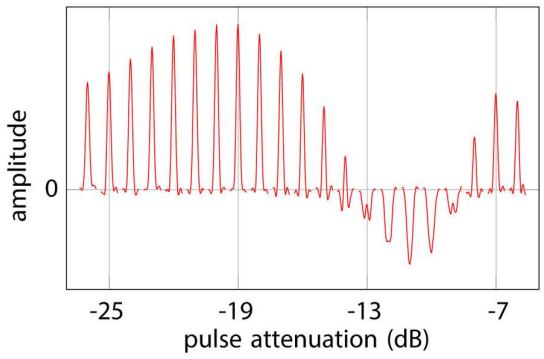

Figure 3 A nutation curve with a pulse duration of 2.5 µs demonstrates a full 360° degree rotation of the spins as the pulse amplitude is increased. The 90° condition, used to measure the NMR signal occurs at the maximum (-19 dB). Echos are formed by applying 180° rotations which occur at -13dB. The powers are attenuated pulse from the spectrometer's 100W RF amplifier

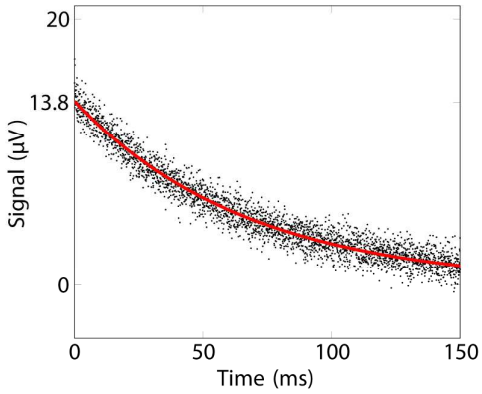

Figure 4 A representative *in vivo* transverse relaxation measurement performed wirelessly on a sensor loaded with the pH sensitive gel. The line represents a fit to a single exponential decay curve. The signal to noise ratio for this experiment is 380. The fitted T_2 = 67.2 ms with a 95% confidence interval of 0.7 ms.

Materials and methods

Sensor fabrication

The sensor is machined from a solid piece of polyether ether ketone (PEEK) on a micromachining center (Cameron Micro Drill Presses). Thin walls form a 10 µL container for the contrast agent and provide a structure on which to wind the coil. The coil consists of 42 turns of polymer-coated 79 µm diameter copper wire (MWS industries). The wires are terminated inside a pocket machined on the end of the sensor. A chip capacitor is soldered inside the pocket to form the resonant circuit. The entire structure is potted in medical-grade epoxy (Hysol Corporation) and cured at room temperature. All sensors were washed in laboratory detergent, rinsed in deionized water, and rinsed in isopropanol before drying. The completed sensor measures 2.2 mm in diameter and 6 mm in length. One sensor was sterilized in a steam autoclave to test for sterilization compatibility.

Reader coil fabrication

The reader coil is 28 mm in diameter and consists of two pairs of turns separated by 14 mm. This configuration is known as a Helmholtz coil and ensures a uniform field in the center and, hence, a relatively constant mutual inductance with the sensor over a volume far greater than the sensor size. The mutual inductance varies by approximately 1% within an 8 mm sphere at the center of the reader coil. This uniformity allows for very crude positioning of the sensor without any loss of tuning. Two variable capacitors, C_T and C_M, (Johanson Manufacturing Corporation) create a resonant probe and are used to transform the impedance at resonance to 50Ω to match the spectrometer's output impedance.

Complete circuit

The circuit is completed by bringing the reader and sensor in close proximity to each other, giving rise to a mutual

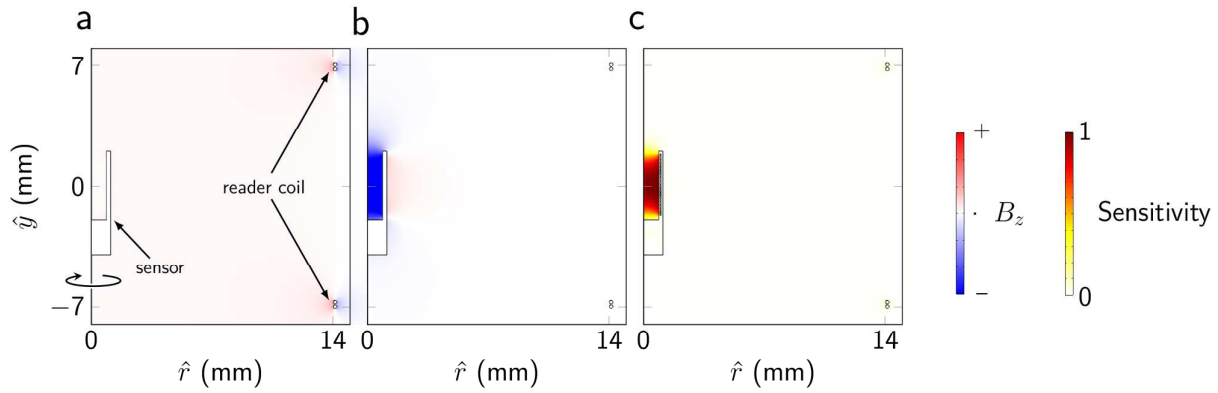

Figure 5 a-b, Numerical simulations in 2-D cylindrical geometry of the sensor centered inside the reader coil. The field shows both real and imaginary decompositions of the y-directed field. The driving current in the reader coil generates a weak field (a), wherease the buildup of field inside the sensor is out of phase and larger in magnitude (b). c, The sensitivity of the NMR experiment as a function of position is a combination of the excitation pulse and the ability of the sensor to detect magnetization from a given position. The nutation angle during the pulse and the induced voltage during reception are both proportional to B_y. The result is that the contents of the sensor are all that are measured.

inductance between their coils. The circuit diagram (Fig. 2) shows the transmitter simplified as a voltage source with an internal resistance. Current flowing through the reader coil, i_R, induces a voltage in the sensor coil,

$$v_S = M\frac{di_R}{dt}$$

via the mutual inductance, M.

The important parameter for NMR experiments is the current in the sensor, i_s, because this gives rise to the oscillating magnetic field needed for the pulses. The spectrometer applies a voltage across the reader coil, v_R, and we need to find the resulting current in the sensor. The transfer function, $Y(\omega)$, is given by

$$Y(\omega) = \frac{I_S}{V_R} = \frac{j\omega M Y_R Y_S}{1 + \omega^2 M^2 Y_R Y_S}$$

where the capital symbols imply a Laplace transform of the corresponding time-domain signals and ω is the frequency. Y_R and Y_S are the admittances, or the inverse impedance, of the reader coil and the sensor respectively[17].

This equation has two regimes with respect to the mutual inductance. As $M \to 0$, $Y(\omega) \propto M$ and increasing M will increase the power transmitted. As M increases and $\omega^2 M^2 Y_R Y_S \gg 1$, then $Y(\omega) \propto 1/M$ and the transmitted power will be reduced. There exists a condition, $\omega^2 M^2 Y_R Y_S = 1$ that maximizes the transmitted power. The same condition also holds for receiving the NMR signal.

Any deviation from the parallel orientation of the sensor and reader will reduce the mutual inductance; a slight overcoupling, therefore, is desired to maintain the signal even with imperfect positioning.

Magnetic resonance measurements

The static magnetic field is provided by a single-sided magnet (Magritek). Measurements are performed with standard pulse sequences on a commercial spectrometer (KEA 2, Magritek). A nutation curve was obtained by applying a 2.5 µs pulse of increasing amplitude and recording the NMR signal (see Fig. 3).

The mutual inductance is expected to be zero if the two coils are perpendicularly oriented. The angular dependence was explored with a 20 MHz sensor inside a magnet with a more homogeneous field (Bruker mq-20, 0.47 T field strength). The sensor was held in a custom-built reader coil with a rotating fixture, and the signal was measured as a function of angle from -60 degrees to +60 degrees from the parallel orientation. The effective transmitted pulse is reduced when the sensor is off-angle, so a nutation experiment (as in Fig. 3) was performed to calibrate pulse amplitude. The received signal is therefore the maximum possible signal for each angle.

Transverse relaxation time, T_2, measurements are acquired using a standard multi-echo pulse sequence. A total of 3,000 echoes spaced 50 µs apart were acquired. Data were averaged over 16 repetitions with 1.25 s between measurements to allow the magnetization to recover to equilibrium. The total measurement time was approximately 30 s. The resulting amplitude data were fit to the equation $I = A \cdot e^{-t/T_2}$ to extract the transverse relaxation time. To ensure high quality data were acquired in vivo each measurement was performed 16 times. A representative example of in vivo data is shown in Fig. 4. The signal-to-noise ratio of the sensors is compared to a commercial benchtop relaxometer (Bruker Minispec mq-20) with a 10 mm diameter NMR tube containing 1 mL of the pH-sensitive gel.

Longitudinal relaxation time, T_1, measurements are performed using a saturation-recovery pulse sequence. The magnetization is saturated with series of irregularly-spaced pulses and measured after recovery towards equilibrium for a time, τ, using a sequence of spin-echo pulses as described above for

measuring transverse relaxation. The signal intensity is recorded at 13 different recovery times and averaged over 4 repetitions. The data of intensity versus recovery time are normalized across the acquisition session and fit to a form:

$$I = A \cdot (1 - e^{-\tau/T_1}).$$

pH sensor fabrication and testing

A mixture of 24% hydroxyethyl methacrylate and 3% bismethacrylamide in deionized water was mixed with a free-radical initiator under oxygen-free conditions. The mixture was transferred into the probe chamber, and the reaction proceeded at room temperature for approximately 16 hours. The probes were then soaked in a saline bath for 24 hours before use.

The sensor was tested *in vitro* in a flow experiment. The sensor was mounted inside a tube carrying saline. The saline bath was approximately 500 mL in volume and maintained at 36°C +/- 1°C. The bath pH was adjusted by adding hydrochloric acid or sodium hydroxide solutions. An electrochemical pH meter (Thermo Fisher) recorded the bath pH to calibrate the sensors. The flow tube with the sensor was positioned inside the reader, and transverse relaxation rate was measured continuously for 25 days.

pH animal model

All animal experiments were conducted under the supervision of the Department of Comparative Medicine and in accordance with the guidelines of the Committee on Animal Care at the Massachusetts Institute of Technology. Four C57/BL6 mice were inoculated subcutaneously with 10^6 melanoma cells derived from the same breed. They were allowed to incubate for 7-10 days forming solid tumors approximately 1 cm in diameter. The sensors were implanted with a biopsy needle, and the wound was closed with tissue glue (3M VetBond). One sensor was implanted in each animal, with each animal receiving the sensor in a different location. One was implanted directly inside the tumor; a second was implanted adjacent to the tumor, and a third was implanted subcutaneously on the contralateral side. One mouse did not have a sensor implanted to ensure that the measurement was of the sensor and not of the mouse.

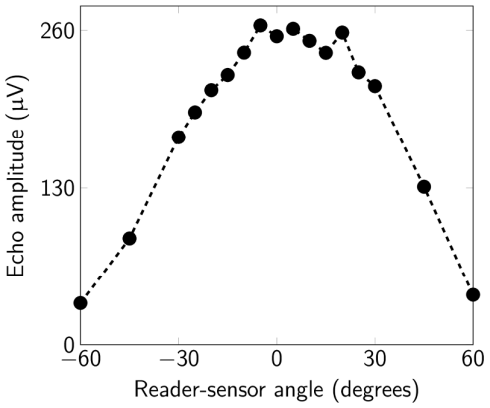

Figure 6 The precise alignment of the sensor relative to the reader is not critical. The angle of the sensor was changed over 120 degrees and the NMR signal amplitude was measured. The changing angle changes the mutual inductance between the two coils resulting in a reduction of signal.

The mice were anesthetized using 2% isofluorane in a balance of oxygen and restrained inside a 26 mm diameter cylinder. The cylinder was inserted into the reader coil and positioned until the sensor was centered in the reader. Although the sensor could not be seen, it was possible to detect when it was at the center based on a measurement of the reader coil impedance.

Oxygen sensor fabrication and testing

Oxygen sensors were made by filling the sensor with a silicone oil embedded in a polymeric matrix that has been shown to give excellent oxygen contrast[14]. A 7:3 mass ratio mixture of liquid dodecamethylpentasiloxane and polydimethylsiloxane (Sylgard 184) with its curing agent were transferred into the sensors. The sensors were cured at 80°C for approximately 1.5 hours.

The sensor was mounted inside a gas flow tube that ran through the reader coil. The oxygen fraction within the gas was controlled and varied between 0% and 20% oxygen in nitrogen. Intensity data were acquired using a saturation recovery sequence at a single recovery time, τ = 600 ms. This fast, T_1-weighted sequence allows monitoring of the sensor dynamics but does not give absolute T_1 values.

Oxygen animal model

A sensor was implanted with a biopsy needle into the calf muscle of a Sprague-Dawley rat. The rat was anesthetized using 2% isofluorane in medical grade oxygen. A small incision was made distally to the implantation site and a diamond-bevel biopsy needle (Stryker) was inserted into the gastrocnemius muscle. The needle was removed to leave the outer cannula through which the sensor was implanted into the muscle. No additional procedure was required to retain the sensor in place, and the incision site was sealed using tissue glue (3M VetBond). The rat was able to move freely immediately after the procedure and showed no signs of distress. The sensor was implanted eight days prior to the measurement, and the implantation wound had completely healed.

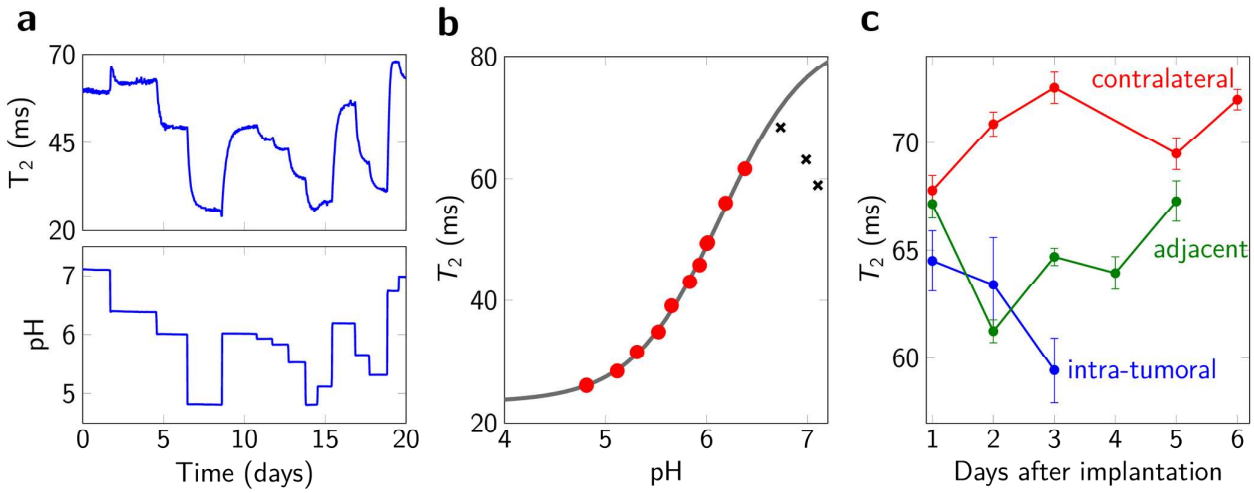

Figure 7 Sensing pH with sensors filled with pH-sensitive gel. The sensor filled with pH sensitive hydroxyethyl methacrylate measured pH of flowing fluid. a, Measured relaxation time over 20 days. **b**, The resulting *in vitro* response curve is valid below pH 6.5, but a second relaxation mechanism is active closer to neutral pH. The error bars are smaller than the sumbols. **c**, Relaxation measurements from three sensors implanted in a mouse melanoma model reveal the more acidic conditions known to exist in tumors. No signal was received from a mouse without a sensor implanted.

The rat was anaesthetized as above and a recirculating water blanket ensured a constant body temperature throughout the experiment. The rat calf was inserted through the reader coil and secured. The T_1 relaxation time measurements were performed periodically to establish a baseline. A nylon cuff, tightened around the thigh, induced an ischemic condition that mimics compressive injury. The cuff was removed following the experiment and the rat was monitored throughout recovery. There were no signs of tissue damage from the restriction, and the rat was completely ambulatory after the measurement.

Histology

The muscle tissue with the implanted device was excised and fixed in 10% formalin solution. The tissue was embedded with methacrylate resin, so that the section could include the entire device. The sample was ground along the axis of the probe and stained with hematoxylin and eosin (CBSET, Inc., Lexington, MA). A bright-field image of the cross section (Fig. 8d) shows the cross section of the probe and the surrounding tissue.

Results and discussion

Device Performance

The sensors used in the experiments had an inductance of 1.3 µH and a quality factor of approximately 40. The fabrication process is very reproducible and a batch of 12 sensors had a resonant frequency standard deviation of 18 kHz or approximately 0.1%. This deviation is an order of magnitude lower than the bandwidth of the sensors, so the sensors are effectively identical.

A nutation experiment shown in Figure 3 shows a 90° condition of -19 dB attenuation of the 100 W amplifier with a pulse duration of 2.5 µs. Inversion of the spins, or the 180° nutation angle, occurs at 6 dB lower attenuation (approximately double the signal strength) as expected.

We compared our sensor's performance to the commercial relaxometer (Bruker mq-20) with a sensitivity metric that takes into account differences in field strength (0.47 T vs 0.37 T), sample size (1 mL vs 10 µL) and number of averages. The sensitivity metric, σ, is defined as:

$$\sigma = \frac{s}{n} \cdot \frac{1}{m\, B_0^2 \sqrt{N}}$$

where s is the signal intensity at $t = 0$, n is the root-mean-squared noise per point, m is the sample mass, B_0 is the field strength, and N is the number of scans. The commercial relaxometer has a sample volume that is 100 times greater (1 mL vs 10 µL) and a magnetic field strength 25% higher than the sensor. The 25% greater field strength has two distinct effects on sensitivity. First, the equilibrium magnetization, M_0, is proportional to the field strength at high temperature. Second, the induced voltage in the coil is determined by the rate of change of the magnetization that is precessing at the Larmor frequency, $\omega = \gamma B_0$. Therefore the signal voltage,

$$v \propto \frac{dM}{dt} = M_0 \frac{d}{dt} \sin \omega t \propto \omega M_0 \propto B_0^2$$

is proportional to the squared magnetic field. Finally, the number of averages, N, increases the SNR by a factor $\sqrt{N}$. Normalizing the sensitivity of the commercial relaxometer to

be σ_n = 1,,we can directly compare the detection sensitivity of the two instruments. The sensors have normalized sensitivity, σ_n= 1.2, slightly above the commercial relaxometer, when tested both *in vitro* and *in vivo* using the single-sided magnet. The same sensors tested in the benchtop relaxometer's magnet for the angular dependence study have a much higher sensitivity, σ_n= 7. The larger value in the benchtop magnet is due to the field homogeneity. The single-sided magnet has a static field gradient that is designed for measuring a thin (~0.5 mm) slice through the sample. This gradient is convenient for testing sensors at different Larmor frequencies but it reduces the effective sample volume. The signal-to-noise ratio can therefore be increased 5-fold by designing a custom magnet with a more homogeneous field.

The key element that determines the success of the sensors is the field amplification inside the chamber that comes from the resonant circuit. This ensures high sensitivity to the contents and simultaneously no sensitivity to the surrounding tissue. The resulting signals originate only from the sensor and none of the surrounding matter even though the tissue inside the reader coil vastly exceeds the sensor volume (approximately 250-fold). The field amplification inside the sensor can be calculated numerically, as shown in Fig. 5, but a first-order approximation given by the quality factor, Q, of the coil.

The resonant circuit also ensures that only the contents of the sensor are measured with negligible interference from the surrounding region. This means the potentially difficult task of locating the sensor is removed from the measurement process. The sensor effectively performs a single-voxel measurement by isolating the measurement to the contents of the sensor. The sensitivity of the measurement to locations around the sensor is shown in Fig. 5c. Signal in the sensor is isolated from the surrounding environment during both excitation and reception. The excitation pulse is programmed to rotate the nuclear magnetization by 90^{O} in the center of the sensor coil. The weaker magnetic field outside the sensor rotates the magnetization by a proportionally smaller angle. The field map also predicts the voltage induced in the reader coil from a unit of magnetization at any point in space. Regions with a stronger field when the reader coil carries one ampere of current induce a proportionally larger voltage in the reader coil [18]. The signal contribution from those regions outside the sensor will be weaker even if the magnetization is equal everywhere. A weaker field during excitation not only results in less excited magnetization but also predicts less efficient detection. These two effects combined virtually eliminate any signal from regions outside of the sensor.

The parallel orientation simulated numerically is not always achievable, however, and the signal is reduced if the sensor and reader are far from parallel (Fig. 6). Small deviations, up to 15^{O}, have little effect due to a slight overcoupling of the reader and sensor. At larger deviations (60^{O}) the signal, although detectable, is too weak for our application.

No change in resonance frequency was observed in the samples washed in soap, water and isopropanol. The single sensor that was also sterilized in a steam autoclave showed no change in resonant frequency and was fully operational after the sterilization process.

pH experiments

Measurements of the gel equilibrated within 24 hours of a change in pH. (Fig. 7a) A calibration curve of sensor relaxation time, $T_{2,}$ versus pH is extracted from the data and reveals a monotonic range between pH 4.8 and pH 6.8 (Fig. 7b). The fitted T_2-versus-pH curve is modeled assuming a single exchangeable hydrogen atom on the polymer chain that follows a pH dependent chemical exchange rate. The error in pH measured by the sensor is calculated with respect to the pH electrode measurement when the gel is equilibrated with the bath. The standard deviation of the error is 0.028 pH units across 1010 measurements.

This particular gel exhibits a second relaxation mechanism above neutral pH that is possibly due to a second exchangeable hydrogen atom on the polymer. A different gel is necessary to monitor changes around normal physiological pH, but our studies were focused on the study of cancer. This property makes the gel suitable for measuring acidic environments, such as tumor response. Cancer cells undergo

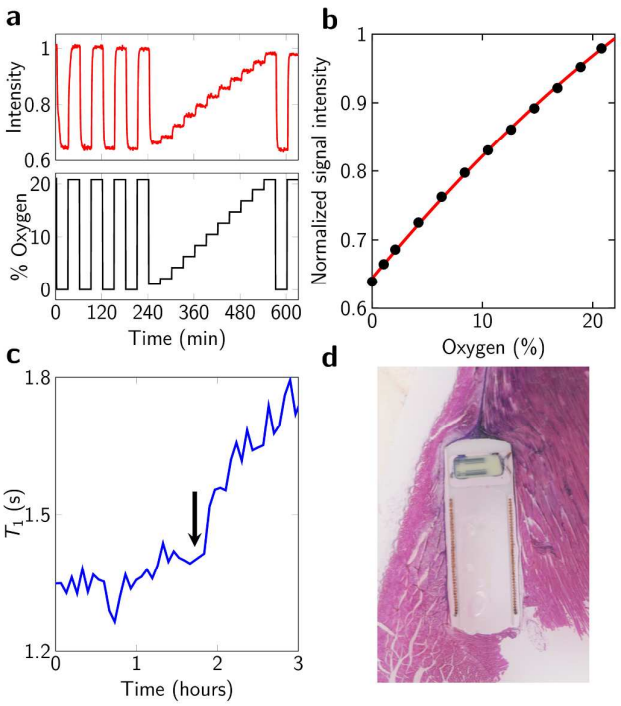

Figure 8 Oxygen sensing in vitro and in a rodent model. a, T1-weighted intensity measurements of a sensor filled with oxygen-sensitive dodecamethylpentasiloxane in a polydimethylsiloxane matrix responds in less than 10 minutes to changes in the oxygen partial pressure in flowing gas. b, The resulting sensitivity versus oxygen fraction in gas. The error bars are smaller than the symbols, c, The longitudinal relaxation time of a sensor, which was implanted in the calf muscle of a rat, shows a marked increased after circulation to the leg was restricted. The arrow indicates the time at which the cuff was tightened. d, A resin-embedded tissue section of the sensor in muscle shows minimal adverse tissue reaction.

anaerobic glycolysis and produce lactic acid as a byproduct[19] which acidifies the environment.

Distinct responses were detected in the three mice with pH sensors implanted. No signal was detectable from the animal without a sensor implanted confirming that no signal outside the sensor is detected directly by the reader coil. The measurements performed over several days with the implanted sensors are shown in Fig. 7c. The signal on the contralateral side shows the highest relaxation time, consistent with a higher pH. The two sensors closer to the tumor show a reduced relaxation time consistent with a pH of approximately 6.5.

Oxygen experiments

The oxygen sensors were measured with a T1-weighted spin-echo sequence as the applied oxygen fraction was changed (Fig. 8a). The high diffusivity of oxygen in the silicone ensures a very rapid response rate, and the measured signal equilibrates within 10 minutes of a change in gas composition. The sensor is reversible over the full range of oxygen fraction, and the resulting signal versus oxygen concentration shows an oxygen sensitivity of better than 10 kPa (Fig. 8b). The relaxation change arises due to the paramagnetism of molecular oxygen, which increases the relaxation rate of the protons in the silicone. There are very few other paramagnetic species in the body, and the hydrophobic nature of silicone makes it very specific to oxygen. Only the proximity of oxygen matters, and there is no reaction taking place, so the sensor will be stable indefinitely *in vivo*.

Oxygen sensors implanted in rats were measured before and after the nylon cuff was tightened. These measurements demonstrated that the sensors measured oxygen tension at the implant site independently of blood flow. The lower oxygen tension caused by a tightening of the cuff is detected as an increase in relaxation time in the latter part of the experiment (Fig. 8c; $p<0.001$). A histological section of the implanted sensor and the surrounding muscle tissue shows little sign of adverse tissue reaction after several weeks of implantation (Fig. 8d). We looked only for gross abnormalities with the H & E stain, but markers for cell death should be explored in future studies.

Conclusions

We have demonstrated a wirelessly-powered sensor utilizing nuclear magnetic resonance. We exploited NMR contrast agents that show a relaxation rate change in response to a target. The two different measurements show the flexibility of this general-purpose NMR probe. The wireless readout offers fast, sensitive readout without any need for imaging and without any interference from surrounding tissue. The sensor could be used to perform other NMR experiments *in vivo*, such as low-resolution spectroscopy to search for soluble biomarkers. The chamber could be filled with an inert matrix to act as a filter and provide a clean, uniform sample to measure. The sensor materials would be selected to eliminate any mismatch in magnetic susceptibility similar to previous work that used inductively-coupled probes for sample spinning[20]. Advances in single-sided magnets that generate a uniform magnetic field [21] combined with miniaturized spectrometer electronics[22] provide promise for spectroscopy-based sensing *in vivo*.

This work offers a very broad platform for wireless sensing inside the body given the broad range of NMR techniques that are available. These implantable labs are remotely powered and, since no internal power source is needed which results in their small dimensions. The analyte target is determined entirely by the contrast agent opening up opportunities for disposable chemical sensors in diverse applications, through opaque and conductive media. We demonstrated the ability to produce sensors with tight tolerances, using off-the-shelf components, even in this early-stage work. The sensors are also inexpensive enough – all of the sensitive electronics are external – that they can be used in applications where the device will ultimately be destroyed such as in chemical reactors. These devices are extremely rugged and have potential for long-term embedding in products or building materials to monitor properties over time.

Acknowledgements

This work was supported by National Cancer Institute Centers of Cancer Nanotechnology Excellence Grant 5U54CA151884-03 and United States Army Research Office Grant W911NF-13-D-0001.

Notes and references

1 J. Pintaske, P. Martirosian, H. Graf, G. Erb, K.-P. Lodemann, C. D. Claussen and F. Schick, *Invest. Radiol.*, 2006, **41**, 213–21.
2 R. Weissleder, *Science*, 2006, **312**, 1168–1171.
3 J. M. Perez, L. Josephson, T. O'Loughlin, D. Hogemann and R. Weissleder, *Nat. Biotechnol.*, 2002, **20**, 816–820.
4 A. Z. Wang, V. Bagalkot, C. C. Vasilliou, F. Gu, F. Alexis, L. Zhang, M. Shaikh, K. Yuet, M. J. Cima, R. Langer, P. W. Kantoff, N. H. Bander, S. Jon and O. C. Farokhzad, *ChemMedChem*, 2008, **3**, 1311–5.
5 Y. Ling, C. C. Vassiliou and M. J. Cima, *Analyst*, 2010, **135**, 2360–2364.
6 S. Taktak, D. Sosnovik, M. J. Cima, R. Weissfeder and L. Josephson, *Anal. Chem.*, 2007, **79**, 8863–8869.
7 P. L. Choyke, A. J. Dwyer and M. V. Knopp, *J. Magn. Reson. Imaging*, 2003, **17**, 509–520.
8 C. F. G. C. Geraldes and S. Laurent, *Contrast Media Mol. Imaging*, **4**, 1–23.
9 J. Rajendran and K. Krohn, *Radiol. Clin. North Am.*, 2005, **43**, 169–187.
10 R. D. Braun, J. L. Lanzen, S. a Snyder and M. W. Dewhirst, *Am. J. Physiol. Heart Circ. Physiol.*, 2001, **280**, H2533–44.
11 Y. Ling, T. Pong, C. C. Vassiliou, P. L. Huang and M. J. Cima, *Nat Biotech*, 2011, **29**, 273–277.

12 K. D. Daniel, G. Y. Kim, C. C. Vassiliou, M. Galindo, A. R. Guimaraes, R. Weissleder, A. Charest, R. Langer and M. J. Cima, *Biosens. Bioelectron.*, 2009, **24**, 3252–3257.
13 K. D. Daniel, G. Y. Kim, C. C. Vassiliou, F. Jalali-Yazdi, R. Langer and M. J. Cima, *Lab Chip*, 2007, **7**, 1288–1293.
14 V. H. Liu, C. C. Vassiliou, S. M. Imaad and M. J. Cima, *Proc. Natl. Acad. Sci. U. S. A.*, 2014, **111**, 6588–93.
15 D. Lindner and D. Raghavan, *Br. J. Cancer*, 2009, **100**, 1287–1291.
16 J. a Bertout, S. A. Patel and M. C. Simon, *Nat Rev Cancer*, 2008, **8**, 967–975.
17 C. C. Vassiliou, PhD Thesis, Massachusetts Institute of Technology, 2013.
18 D. I. Hoult and R. E. Richards, *J. Magn. Reson.*, 1976, **24**, 71–85.
19 D. Hanahan and R. A. a Weinberg, *Cell*, 2011, **144**, 646–674.
20 D. Sakellariou, G. Le Goff and J.-F.-F. Jacquinot, *Nature*, 2007, **447**, 694–697.
21 J. Perlo, V. Demas, F. Casanova, C. a Meriles, J. Reimer, A. Pines and B. Blümich, *Science*, 2005, **308**, 1279.
22 N. Sun, T.-J. Yoon, H. Lee, W. Andress, R. Weissleder and D. Ham, *IEEE J. Solid-State Circuits*, 2011, **46**, 342–352.